Proceedings of 10th International Conference on Precision, Meso, Micro and Nano Engineering (COPEN 10)
December 07 – 09, 2017, Indian Institute of Technology Madras, Chennai – 600 036 INDIA

An atomistic simulation based investigation on the influence of Zr addition on deformation behavior of nanocrystalline Ni

Md. Meraj, B. S. K. Gargeya, K.Vijay Reddy and Snehanshu Pal*

Department of Metallurgical and Materials Engineering
National Institute of Technology Rourkela, Rourkela- 769008, Odisha, INDIA

Abstract

The effects of solid solution on the strength and occurrence of fracture of nanocrystalline (NC) Ni and Ni-Zr alloy having average 7 nm grain sizes are investigated using molecular dynamics simulations with embedded atom method potential. The tensile deformation of NC Ni with Zr as solutes present in two different fashions (randomly distributed in specimen and segregated at grain boundary (GB) has been performed for different temperatures at constant strain rate (10^8 s^{-1}). It is found that addition of Zr causes enhancement in the strength and ductility as compared to NC Ni. In addition to that, increase in population fraction of Hirth and stair-rod partial dislocations aided in the increased UTS in Ni-Zr alloy. Intergranular fracture has been found to be delayed for NC Ni-Zr alloy.

Keywords: Molecular dynamics simulation, Plastic deformation, Intergranular crack, Grain boundary segregation, Solid solution strengthening.

1. INTRODUCTION

Nanocrystalline (NC) materials have a wide application, because they have better physical, chemical, mechanical and magnetic properties [1,2]. NC materials are single- or multi-phase polycrystalline solids having grain size in the range of 1 nm – 100 nm [3]. These materials possess higher strength at room temperature when compared to its coarse grained counterpart due to the presence of larger volume fraction of grain boundaries (GBs) and triple junctions [4]. According to the Hall-Petch relationship, the yield stress of materials increases as the grain size decreases from 250 nm to 25 nm [5]. With further reduction in grain size below a critical value (i.e. ~ 20–25 nm, which is also found to be dependent on the nature of the material [6]), the yield stress is started to decrease [7]. This phenomenon is known as the "inverse Hall-Petch effect", and has also been reported in literature studies [8]. Enhancement of ductility [9] and strength [10] in case of NC materials is because of the transition from the dislocation mediated to grain boundary mediated deformation process [11,12,13]. The GB mediated phenomena such as GB sliding [14], GB diffusional creep [15], triple junction diffusion creep [16] and rotational deformation [17] are prevalent mechanisms associated with the deformation of NC materials. Introduction of solute particles in NC metals is found to suppress the grain growth of NC metals [18]. Schäfer et al. have performed MD simulations and found that solute particles reduce the GB energies and thus decrease the driving force for grain growth [19]. The presence of solute particles as either segregated at GB [20] or randomly distributed [21] has significant influence on the strength of the NC material. Tensile deformation behavior of NC Ni having different grain size such as 40 nm [22], 12 nm [23], 30 nm [24] and 20-200 nm [25] are studied experimentally on a micro-sized specimen. It is revealed that flow stress of NC Ni has positive strain-rate sensitivity [22] and NC Ni exhibit local plasticity [24]. The high strength and ductility of NC are significantly influenced by grain refinement and restriction of grain boundary sliding by solute carbon atoms [26]. Apart from carbon atoms, presence of refractory material such as Zr in nanocrystalline material is known to inhibit grain growth and also enhance the strength at high temperature [27,28]. Few experimental studies have been performed to study the influence of Zr in Fe-base alloys [27,28]. In another experimental study, Zhang et al. have determined the mechanical properties of NC Cu-Zr alloy (Zr segregation at GB in Cu) and it has been revealed that strength is enhanced with the addition of Zr at the cost of ductility [29]. However, experimental investigations are very difficult and time consuming to perform at nanoscale level. For instance, in case of TEM analysis, sample preparation is difficult as the sample size is very small and hampers the grain boundary structure, thus giving erroneous results [30]. Moreover, the cost and time required to perform experiments at nanoscale level is very high [31,32]. To understand the variation in mechanical properties of NC metal due to second metal addition, MD simulation can be beneficial tool which can contribute towards detecting the mechanisms involved in the plastic deformation processes [33]. The high temperature deformation of NC Ni-Zr alloy is investigated by MD simulation and it is reported that creep resistance is enhanced by addition Zr atom in NC Ni [34,35].

Zhang et al. have performed tensile tests on bicrystal Cu at 10K and revealed that the dislocations are emitted from the grain boundaries [36]. The role of dislocation controlled mechanism under tensile deformation for NC Al having grain size in the range from 20 to 70 nm [37] is reported using MD simulation. MD simulation is also implemented to investigate the strain rate sensitivity of NC Cu having grain size ranging between 3.8 to 27.3 nm [38]. Cao and Wei [39] have studied the crack nucleation and intergranular fracture through MD simulations in bulk NC Ni which is deformed through the dynamic cyclic uniaxial tensile deformation. The MD simulation of Ni single crystal is performed to understand the deformation and fracture behavior during tension as reported in literature [40]. The deformation behavior of NC Ni nanowires having grain size 7 nm is studied during indentation and tension process using MD simulation and it is reported that GB sliding

*Corresponding author.
Email addresses: pals@nitrkl.ac.in, snehanshu.pal@gmail.com (Snehanshu Pal)

ISBN: 978-93-80689-28-9

and GB mediated dislocation emission are the mechanisms responsible for deformation [41]. To sum up, however some scattered attempts have been made previously to study the effect of solute atoms on deformation feature of NC Ni and Ni-Zr alloy, detailed and coherent study on tensile deformation behavior of NC Ni with varying solute elements in two different fashions such as solute atoms randomly distributed and segregated at GB with different temperatures is still due. The influence of presence of solute atoms (like Zr) on tensile properties and deformation characteristics of NC Ni for three different temperatures (i.e. 100K, 300K and 600K) has been studied in this paper using molecular dynamics simulation.

2. COMPUTATIONAL DETAILS

A cubic specimen of NC Ni has been prepared via the Voronoi construction [42] using AtomEye software [43] to study the tensile deformation of NC Ni, Ni-3 at. % Zr alloy. Zr solute atoms are distributed in the specimen in two different ways such as random distribution and segregation at grain boundaries as shown in **Fig. 1**. Each specimen contains 8 grains with random orientation centered at random positions in the simulation box. The specimens have an average grain size of 7 nm and the simulation box of 14 nm × 14 nm × 14 nm size is taken. The total number of atoms present in the simulation box is equal to 254,188.

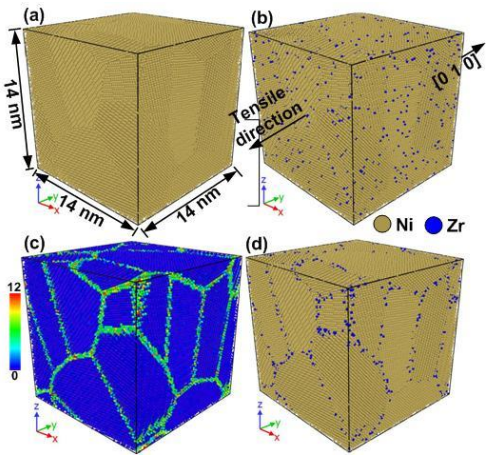

Fig. 1. Three dimensional atomic configuration snapshots for (a) NC Ni, (b) NC Ni-3 at. % Zr(r) alloy, (c) NC specimen according to CSP and (d) NC Ni-3 at. % Zr(s) alloy.

Conjugate Gradient Algorithm is used for energy minimization the specimen at different temperatures (e.g.100 K, 300 K and 600 K) and subsequently simulated tensile test is performed at these temperatures. Time step of 0.002 ps is taken and periodic boundary conditions are applied in all three directions for performing the tensile test simulations. Uniaxial tensile loading is applied along Y-direction (010) with a constant strain rate of 10^8 s^{-1}, while keeping zero loads on the other two directions (i.e. X- and Z- directions). The concentration of alloying element in the specimen is considered to be 3 at. %. Hereinafter, the NC alloys with GB segregations are designated as Ni–Zr(s), while substitutional solid solutions with randomly distributed alloying elements are denoted as Ni–Zr(r). For MD simulations, LAMMPS [44] package has been used with an embedded atom method (EAM) potentials developed by Mendelev et al. [45] and Wilson and Mendelev [46] which is applicable for Ni and Ni-Zr system respectively. OVITO software platform [47] has been used in the analysis of the tensile deformation which includes Wigner-Seitz defect analysis, Dislocation analysis (DXA), Common neighbor analysis (CNA), Centro-symmetry parameter (CSP) analysis, and Cluster analysis. CNA has been performed to identify the structural change in motifs during the tensile loading deformation of NC Ni, Ni-Zr(s) and Ni-Zr(r) specimens. CSP has been used to determine the local lattice disorder in the specimen during tensile loading deformation [48]. For a perfect specimen, the value of the CSP is equal to zero, and the value of CSP is large for plastically deformed defective specimen. The CSP is sensitive to the random thermal displacement of atoms [49]. Wigner–Seitz defect analysis [50] has been carried out for the investigation of vacancies generation during the tensile loading. Wigner–Seitz cell method is an effective tool for identifying the point defects. It identifies the displaced position of the atoms with respect to perfect crystal structure as a reference. Identification of dislocations generated during the tensile loading deformation has been performed by DXA. This method identifies different dislocations along with its burger vector by representing dislocated atoms in a form of a line [51].

3. RESULTS AND DISCUSSION

MD simulations of tensile deformation behavior for NC Ni having Zr additions in two different fashions (i.e. solutes atoms randomly distributed and segregated at GB in the specimen) are reported here. Deviation in maximum stress for different temperature of ~7nm grain size NC Ni due to the additions of Zr in two different fashions has been critically investigated. The influence of structural changes of specimen on formation of cluster, vacancy and dislocation evolution has been studied during tensile loading.

3.1. Influence of Zr addition on stress-strain behavior of NC Ni and fracture under tensile loading

The stress-strain curves of NC Ni having 3 at. % of Zr addition distributed in random fashion and segregated at GB is presented in **Fig. 2.** The plots show that the stress-strain curves increase till ultimate tensile stress (UTS). Once UTS is reached, the stress-strain plot shows a steep drop which is attributed to the reduction in flow stress, and then the curves decrease gradually up to fracture. The decrease of stress after UTS shows a zigzag pattern which indicates that strain hardening is operative at this stage of deformation process. It is observed that yield strength and UTS are enhanced with addition of Zr atoms in NC Ni specimen when compared with pure NC Ni specimen. This is because of higher resistance to coupled GB motion due to the presence of solutes [52]. This is attributed to the fact that, for nanocrystalline solids with grain size less than ~15 nm, it has been found that solute atom which stiffens the lattice helps in increasing the strength of the material [21]. Mechanical properties obtained from stress-strain curves such as yield strength, Young's modulus, UTS are plotted vs. temperature in **Fig. 3** to show the influence of temperature on the mechanical properties of NC Ni and Ni-Zr alloy. It is observed that the yield stress and Young's modulus (which is obtained from the slope of the stress–strain curves near zero strain) decreases gradually as temperature increases from 100 K to 600 K, shown in **Fig. 3 (a)** and **Fig. 3 (b)** respectively.

It is observed from **Fig. 3(c)** that the ultimate tensile strength (UTS) is decreased monotonically with increasing temperature from 100 K to 600 K for all the specimens studied here. The decrease in UTS with temperature is attributed to the softening phenomena occurring with increasing temperature during tensile loading deformation. Overall, the UTS of NC Ni is increased with addition of Zr atoms as evident in **Fig. 3(c)**.

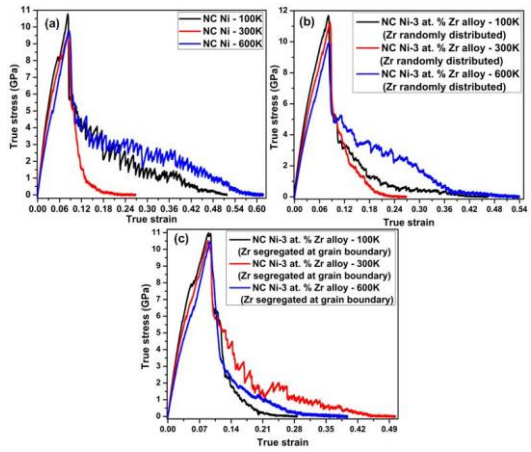

Fig. 2. True stress-strain curves for (a) NC Ni, (b) NC Ni-3 at. % Zr(r) alloy and (c) NC Ni-3 at.% Zr(s) alloy at three different temperatures.

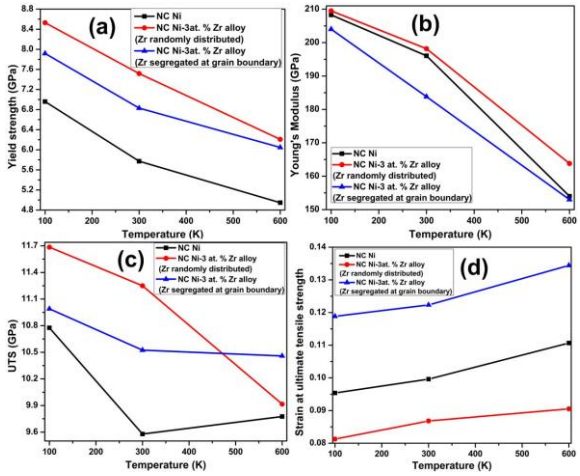

Fig. 3. Plots of (a) yield strength vs. temperature, (b) Young's modulus vs. temperature, (c) ultimate tensile strength vs. temperature and (e) Strain at ultimate tensile strength vs. temperature.

Fig. 3(d) represents the strain at UTS vs. temperature plots for NC Ni and Ni-Zr alloys. It is observed that strain at UTS for NC Ni and Ni-Zr alloys are found to increase as the temperature is increased. It is due to the softening of the specimen which results in enhancement of ductility with increasing temperature during tensile loading. It is also observed that strain at UTS is enhanced with addition of Zr atoms in all the specimens having randomly distributed and segregated at grain boundary except NC Ni-Zr(r) for different temperature. Atomic snapshots of all the nanocrystalline specimens at 300 K for four different stages of strain are shown in **Fig. 4.** The atoms are colored according to the CSP for NC Ni and NC Ni-Zr alloy at 300 K temperature. The snapshots shows that several different deformation mechanisms are activated such as nanotwin formation, grain boundary sliding, intergranular crack origination and fracture during tensile deformation. It is observed in **Fig. 4** that cracks have been originated at intergranular region for all cases during tensile deformation. It is because when a dislocation is absorbed by GBs, a stress concentration develops at the absorbing site and a potential crack is nucleated [53].

Intergranular cracks originated at 11, 9 and 13% strain for NC Ni, Ni-Zr(r) and Ni-Zr(s) respectively. It is then propagated with increasing strain and finally the fracture occurred at 27, 27 and 50% strain for NC Ni, Ni-Zr(r) and Ni-Zr(s) respectively.

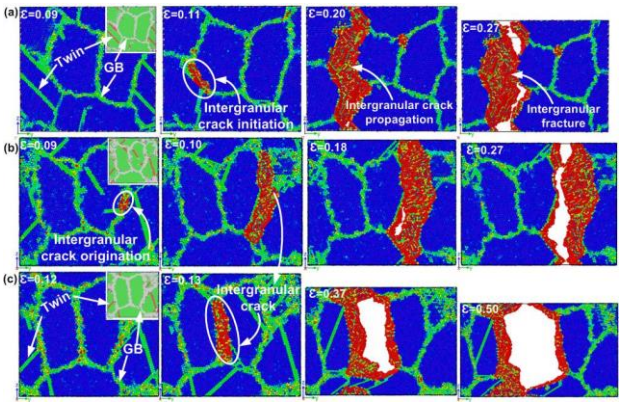

Fig. 4. Atomic snapshots of the nanocrystal at four different stages of strain for (a) NC Ni, (b) NC Ni-3 at. % Zr(r) alloy and (c) NC Ni-3 at.% Zr(s) alloy at 300 K temperature. Atomic snapshot of crystal structure according to CNA is given in inset.

It is observed that the intergranular fracture occurs along the grain boundary perpendicular to the loading direction. Propagation of an intergranular fracture in the presence of an existing crack is reported in literature by MD simulations on NC Ni [54]. Here, however, the intergranular crack nucleation is influenced by only the applied strain in the presence of the grain boundary. Similar finding has also been reported in literature for NC Mo using MD simulation [55]. The intergranular nucleation and fracture is found to be delayed for NC Ni-Zr(s) alloy specimens as compared to NC Ni specimen at 300 K temperature, as evident from **Fig. 4**. **Table 1** provides the fracture strain during deformation at different temperatures for all the specimen. It has been found that NC Ni fractures at higher strain during 100 K and 600 K deformation.

Table 1: Fracture strain for different specimens and temperatures

Specimen type	True strain at the point of fracture		
	100 K	**300 K**	**600 K**
NC Ni	0.52	0.27	0.62
NC Ni-3 at. % Zr (Zr randomly distributed)	0.46	0.27	0.54
NC Ni-3 at. % Zr (Zr segregated at GB)	0.28	0.50	0.40

Cluster analysis has been performed by considering the cut off radius range of 2.45 Å to 2.50 Å, as per the first peak of the RDF plots. Numbers of clusters vs. true strain plots at different temperatures (i.e. 100 K, 300 K and 600K) are presented in **Fig. 5**. It is observed that with increase in strain, number of clusters increased initially and then dropped suddenly followed by gradually decrease up to fracture for all cases. The increase in number of clusters indicates the formation of twins in the specimen [56]. The peak of clusters formation curves is shifted downward with increasing temperature for all specimens as similar trend is also followed during stress-strain curves. Comparing **Fig. 2** and **Fig. 5**, we can say that maximum number of clusters is formed at the point of maximum stress and its values decreases with the increase of temperature. From **Fig. 5**, it is evident that maximum number of cluster formation is for NC Ni-Zr(s) at all temperature followed by Ni-Zr(r), and the least number of clusters is for NC Ni.

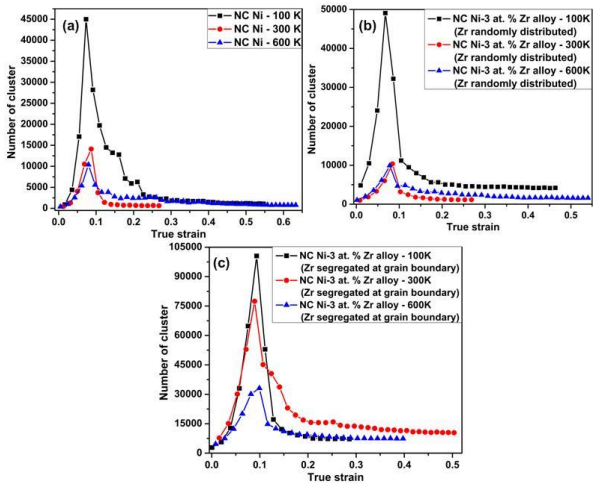

Fig. 5. Plots of number of cluster vs. true strain for (a) NC Ni, (b) NC Ni-3 at. % Zr(r) alloy and (c) NC Ni-3 at. % Zr(s) alloy at three different temperatures.

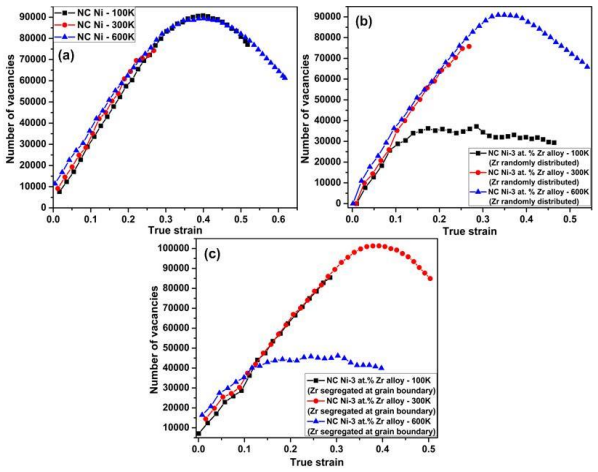

Fig. 6. Plots of number of vacancies vs. true strain for (a) NC Ni, (b) NC Ni-3 at. % Zr(r) alloy and (c) NC Ni-3 at. % Zr(s) alloy at three different temperatures.

Number of vacancies generated vs. true strain plots under tensile loading for NC Ni and Ni Zr alloys are presented in **Fig. 6**. Number of generated vacancies increases up to certain value of strain, then decreases with increasing strain, as evident from **Fig. 6**. The vacancies shifted upward with increasing temperature during tensile loading for almost all cases of NC specimens. It is also observed that for NC Ni-Zr(s), number of vacancies formation is decreased after 11.62 % strain and shifted downward at 600 K as compared to 100 K and 300 K temperature as shown in **Fig. 6(c)**. Maximum number of vacancies generation occurred more in NC Ni-Zr(s) specimen at 300 K temperature.

3.2. Influence of Zr addition on generation of dislocation type of NC Ni under tensile loading

The dislocation density during deformation under tensile loading conditions has been presented for NC Ni and NC Ni-Zr alloy at 100, 300 and 600 K in **Fig.7**. Dislocation density of NC Ni and NC Ni-Zr alloy initially shifts downward with increase in temperature due to increasing diffusivity with the increase in temperature.

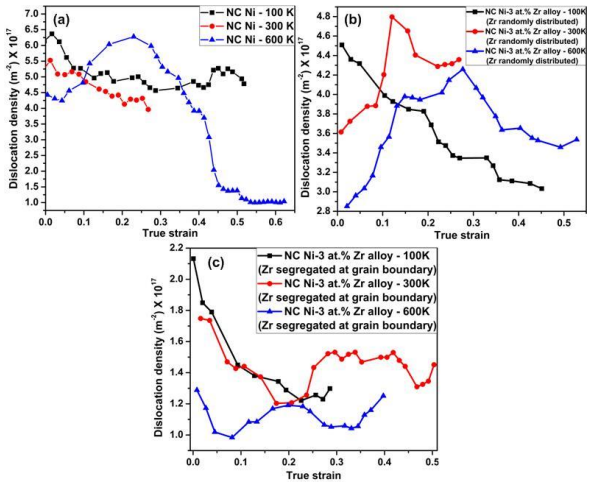

Fig. 7. Plots of evaluated dislocation density vs. true strain for (a) NC Ni, (b) NC Ni-3 at. % Zr(r) alloy and (c) NC Ni-3 at.% Zr(s) alloy at three different temperatures.

From **Fig. 7(a),** it is observed that dislocation density of NC Ni decreases with increase in strain for 100 K and 300 K temperatures, but dislocation density for 600 K temperature initially increased from 5 % strain to 22 % strain and then decreases up till fracture. This is because of strain hardening which occurred more in NC Ni at 600 K temperature, as evident from **Fig. 2 (a)**. Dislocation density of NC Ni-Zr(r) is observed to increase up to a certain point of strain after which it decreases up to fracture for 300 K and 600 K temperatures. It is attributed to the annihilation of dislocations which results in decrease in dislocation density. On the other hand, dislocation density of NC Ni-Zr(r) is decreased from initial point of strain to fracture only for 100 K temperature, as shown in **Fig. 7(b)**. Due to the higher amount of dislocations in the range of ~0.12 - 0.35 strain, more strain hardening occurs in case of NC Ni-3 at. % Zr (r) specimen at 600 K. Therefore, in this case more amount of stress is observed to be required for occurring same amount of deformation (refer **Fig. 2(b)**). Dislocation density for NC Ni-Zr(s) is first decreased, after which it has increased and again decreased with increasing strain for different temperature due to quasi-stationary balance between dislocations slip and grain boundary (GB) accommodation mechanisms [57], as shown in **Fig. 7(c).** In the case of NC Ni-3 at. % Zr(s), dislocation density of specimens deformed at 100 K and 600 K temperature become almost same after the UTS (refer **Fig. 7(c)**). Correspondingly, the stress strain curve also shows a similar decreasing trend after UTS (refer **Fig. 2(c)**). The population fraction of different types of dislocation (such as Stair-rod, Hirth partial, and Frank partial) at the UTS point under tensile loading conditions has been shown for NC Ni and Ni-Zr alloy at 100, 300 and 600 K temperatures in **Fig. 8**.

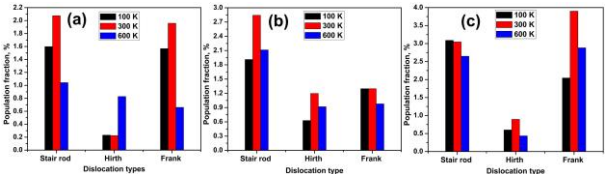

Fig. 8. Plots of population fraction vs. dislocation type at the UTS point for (a) NC Ni, (b) NC Ni-Zr(r) alloy and (c) NC Ni-Zr(s) alloy at three different temperatures.

The presence of Frank partials initiates the cavity formation which in turn leads to fracture of the specimen. Whereas Stair-rod and Hirth partial cause locking of dislocations leading to

strain hardening. In NC-Ni, the population fraction of Frank partial dislocations is higher during tensile deformation at 300 K followed by 100 K and 600 K temperatures as evident from **Fig. 8(a).** This indicates an early failure of the specimen during deformation at 300 K followed by 100 K and 600 K which can be validated from stress-strain curve in **Fig. 2(a).** The presence of high population fraction of Frank partial dislocations in Ni-Zr(s) alloy (as shown in **Fig. 8(c)**) results in an early failure of the specimen. **Fig. 9** shows the variation in Frank partial density after UTS with respect to strain at 300 K temperature for all the specimens. It is observed that at initial strain value (~0.06 strain), Frank partial density is the lowest for NC Ni-3 at. % Zr (r) specimen. But with increase in strain value, the Frank partial density increases rapidly for NC Ni-3 at. % Zr (r) specimen and reaches a maximum at ~0.12 strain. On the other hand, the density of Frank partial dislocations in NC Ni-3 at. % Zr(s) shows a decreasing trend. It is known that the presence of Frank dislocations assists in void and crack formation which leads to fracture of the specimen [58,59]. This phenomenon is also observed in this study as the crack is first initiated in NC Ni-3 at. % Zr (r) specimen at 300 K due to the presence of higher density of Frank partial dislocation density with respect to other specimens (as seen in **Fig. 4**).

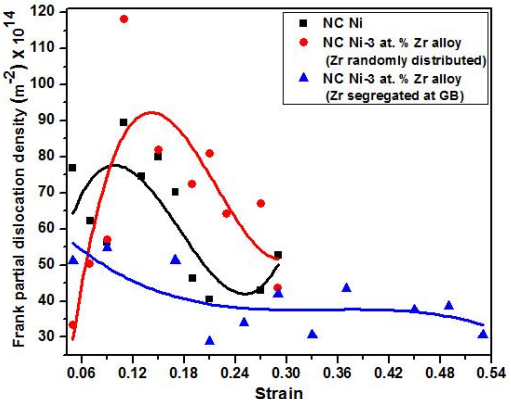

Fig. 9. Plots of Frank partial dislocation density vs. strain for NC Ni, NC Ni-3 at. % Zr(r) alloy and NC Ni-3 at. % Zr(s) alloy at 300 K temperature.

Variation of local crystal structure under tensile loading conditions is identified using common neighbor analysis (CNA). The fractions of different crystal structures present in specimen during deformation under tensile loading conditions for NC Ni and Ni-Zr alloy at 100, 300 and 600 K has been shown in **Fig. 9**. It is observed that the fraction of FCC atoms decreases up to the point of maximum stress and then increases up to the fracture point with progress of deformation. The fractions of HCP and other (disordered) atoms increase up to the point of maximum stress and then decrease up to the fracture point with progress of deformation under tensile loading conditions. This can be attributed to formation of nanotwins (represented as HCP structure in CNA) which helps in retaining the plasticity up to UTS. Once UTS is reached, the fracture mechanism initiates resulting in decrease of HCP structures [60]. The fraction of FCC atoms is shifted downward with increasing temperature, whereas the fraction of HCP and other atoms is shifted upward with increasing temperature under tensile loading conditions.

This is because diffusion is enhanced with the increase in temperature and consequently structural change becomes faster for higher temperature under tensile loading conditions. On the other hand, the fraction of crystal structures is found to be almost constant after ~0.14 strain at 100 K temperature for NC Ni specimen, as shown in **Fig. 9(a)**. The fraction of HCP atoms increased for NC Ni-Zr alloy as compared to the NC Ni system, The HCP structure indicates the twins and stacking faults. The generation of HCP structure can also be validated through cluster analysis in **Fig. 5**.

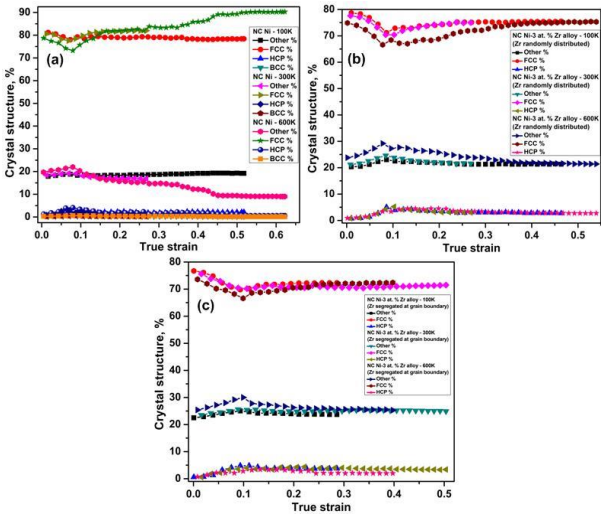

Fig. 10. Plots of crystal structure vs. true strain for (a) NC Ni, (b) NC Ni-3 at. % Zr(r) alloy and (c) NC Ni-3 at. % Zr(s) alloy at three different temperatures.

4. CONCLUSIONS

MD simulations of tensile tests for NC Ni and Ni-Zr alloys have been carried out in this study to investigate the influence of Zr solute addition on the mechanical properties of NC Ni specimen. The following conclusions can be drawn:

- Yield strength and UTS are enhanced with addition of Zr atoms in NC Ni specimen having randomly distributed and segregated at grain boundary.
- Young's modulus is increased with increasing of yield strength during tensile loading for NC Ni and Ni-Zr alloy.
- Ultimate tensile strength (UTS) is decreased monotonically with increasing temperature from 100 K to 600 K temperature for NC Ni and Ni-Zr alloy.
- Increase of dislocation density after UTS causes strain hardening in the NC Ni-3 at. % Zr(r) specimen.
- Cracks are originated at intergranular region at 300 K for a strain value of 0.11, 0.10 and 0.13 for Ni NC, Ni-Zr(r) and Ni-Zr(s) respectively.
- The intergranular nucleation and fracture are found to be delayed for NC Ni-Zr(s) specimens as compared to NC Ni and Ni-Zr(r) specimen at 300 K temperature.
- Early fracture occurs in NC Ni-3 at. % Zr(r) at 300 K because comparatively higher amount of Frank partial dislocations are present.

Acknowledgments

The authors want to thank the computer centre of National Institute of Technology Rourkela for providing high-performance computing facility (HPCF) required for performing this study.

References

[1] Singha, R. K., Shukla, A., Yadav, A., Adak, S., Iqbal, Z., Siddiqui, N., Bal, R., Energy efficient methane tri-

reforming for synthesis gas production over highly coke resistant nanocrystalline Ni–ZrO2 catalyst, *Applied Energy*, **178** (2016) 110-125.

[2] Ul-Hamid, A., Dafalla, H., Quddus, A., Saricimen, H., Al-Hadhrami, L. M., Microstructure and surface mechanical properties of pulse electrodeposited nickel, *Applied Surface Science*, **257** (2011) 9251-9259.

[3] Suryanarayana, C., Koch, C. C., Nanocrystalline materials–Current research and future directions, *Hyperfine Interact*, **130** (2000) 5-44.

[4] Gleiter, H., Nanostructured materials: basic concepts and microstructure. *Acta Materialia*, **48** (2000) 1-29.

[5] Hahn, E. N., Meyers, M. A., Grain-size dependent mechanical behavior of nanocrystalline metals, *Materials Science and Engineering A*, **646** (2015) 101-134.

[6] El-Sherik, A. M., Erb, U., Palumbo, G., Aust, K. T., Deviations from Hall-Petch behaviour in as-prepared nanocrystalline nickel, *Scripta Metallurgica et Materialia*, **27** (1992) 1185-1188.

[7] Chokshi, A. H., Rosen, A., Karch, J., Gleiter, H., On the validity of the Hall-Petch relationship in nanocrystalline materials, *Scripta Metallurgica*, **23** (1989) 1679-1683.

[8] Nieh, T. G., Wang, J. G., Hall–Petch relationship in nanocrystalline Ni and Be–B alloys, *Intermetallics*, 13 (2005) 377-385.

[9] Kim, B. N., Hiraga, K., Morita, K., Sakka, Y., A high-strain-rate superplastic ceramic, *Nature* **413** (2001) 288-291.

[10] Nesladek, P., Vepřek, S., Superhard nanocrystalline composites with hardness of diamond, *Physica Status Solidi A*, **177** (2000) 53-62.

[11] Yip, S., Nanocrystals: the strongest size, *Nature*, **391** (1998) 532-533.

[12] Shan, Z., Stach, E. A., Wiezorek, J. M. K., Knapp, J. A., Follstaedt, D. M., Mao, S. X., Grain boundary-mediated plasticity in nanocrystalline nickel, *Science*, **305** (2004) 654-657.

[13] Schiøtz, J., Jacobsen, K. W., A maximum in the strength of nanocrystalline copper, *Science*, **301** (2003) 1357-1359.

[14] Fedorov, A. A., Gutkin, M. Y., Ovid'ko, I. A., Transformations of grain boundary dislocation pile-ups in nano-and polycrystalline materials, *Acta Materialia* **51** (2003) 887-898.

[15] Yamakov, V., Wolf, D., Phillpot, S. R., Gleiter, H., Grain-boundary diffusion creep in nanocrystalline palladium by molecular-dynamics simulation, *Acta Materialia* **50** (2002) 61-73.

[16] Fedorov, A. A., Gutkin, M. Y., Ovid'ko, I. A., Triple junction diffusion and plastic flow in fine-grained materials, *Scripta Materialia*, **47** (2002) 51-55.

[17] Ovid'ko, I. A., Deformation of nanostructures, *Science*, **295** (2002) 2386-2386.

[18] Detor, A. J., Schuh, C. A., Grain boundary segregation, chemical ordering and stability of nanocrystalline alloys: Atomistic computer simulations in the Ni–W system, *Acta Materialia*, **55** (2007) 4221-4232.

[19] Schäfer, J., Ashkenazy, Y., Albe, K., Averback, R. S., Effect of solute segregation on thermal creep in dilute nanocyrstalline Cu alloys, *Materials Science and Engineering: A*, **546** (2012) 307-313.

[20] Vo, N. Q., Schäfer, J., Averback, R. S., Albe, K., Ashkenazy, Y., Bellon, P., Reaching theoretical strengths in nanocrystalline Cu by grain boundary doping, *Scripta Materialia*, **65** (2011) 660-663.

[21] Rupert, T. J., Solid solution strengthening and softening due to collective nanocrystalline deformation physics, *Scripta Materialia*, **81** (2014) 44-47.

[22] Baek, D. C., Lee, S. B., Fatigue behavior of electrodeposited nanocrystalline nickel films, Procedia Engineering, **10** (2011) 3006-3011.

[23] Yim, T. H., Yoon, S. C., Kim, H. S., Tensile properties of electrodeposited nanocrystalline nickel, *Materials Science and Engineering: A*, **449** (2007) 836-840.

[24] Kumar, K. S., Suresh, S., Chisholm, M. F., Horton, J. A., Wang, P., Deformation of electrodeposited nanocrystalline nickel, *Acta Materialia*, **51** (2003) 387-405.

[25] Schwaiger, R., Moser, B., Dao, M., Chollacoop, N., Suresh, S., Some critical experiments on the strain-rate sensitivity of nanocrystalline nickel, *Acta Materialia*, **51** (2003) 5159-5172.

[26] Kihara, Y., Nagoshi, T., Chang, T. F. M., Hosoda, H., Sato, T., Sone, M., Tensile behavior of micro-sized specimen fabricated from nanocrystalline nickel film, *Microelectron Engineering*, **141** (2015) 17-20.

[27] Kotan, H., Darling, K. A., Saber, M., Koch, C. C., Scattergood, R. O., Effect of zirconium on grain growth and mechanical properties of a ball-milled nanocrystalline FeNi alloy, *Journal of Alloys and Compounds*, **551** (2013) 621-629.

[28] Darling, K. A., VanLeeuwen, B. K., Koch, C. C., Scattergood, R. O., Thermal stability of nanocrystalline Fe–Zr alloys, *Materials Science and Engineering: A*, **527** (2010) 3572-3580.

[29] Zhang, P., Zhang, J. Y., Li, J., Liu, G., Wu, K., Wang, Y. Q., Sun, J., Microstructural evolution, mechanical properties and deformation mechanisms of nanocrystalline Cu thin films alloyed with Zr, *Acta Materialia*, **76** (2014) 221-237.

[30] Van Swygenhoven, H., Grain boundaries and dislocations, *Science*, **296** (2002) 66-67.

[31] Komanduri, R., Chandrasekaran, N., Raff, L. M., Molecular dynamics (MD) simulation of uniaxial tension of some single-crystal cubic metals at nanolevel, *International Journal of Mechanical Sciences*, **43** (2001) 2237-2260.

[32] Chang, W. J., Fang, T. H., Influence of temperature on tensile and fatigue behavior of nanoscale copper using molecular dynamics simulation, *Journal of Physics and Chemistry of Solids*, **64** (2003) 1279-1283.

[33] Li, J., Liu, B., Luo, H., Fang, Q., Liu, Y., Liu, Y., A molecular dynamics investigation into plastic deformation mechanism of nanocrystalline copper for different nanoscratching rates, *Computational Materials Science*, **118** (2016) 66-76.

[34] Pal, S., Meraj, M., Deng, C., Effect of Zr addition on creep properties of ultra-fine grained nanocrystalline Ni studied by molecular dynamics simulations, *Computational Materials Science*, **126** (2017) 382-392.

[35] Meraj, M., Pal, S., Effect of temperature and stress on creep behavior of ultrafine grained nanocrystalline Ni-3

at% Zr alloy, *Metals and Materials International*, **23** (2017) 272-282.

[36] Zhang, L., Lu, C., Tieu, K., Pei, L., Zhao, X., Cheng, K., Molecular dynamics study on the grain boundary dislocation source in nanocrystalline copper under tensile loading, *Materials Research Express*, **2** (2015) 035009.

[37] Yamakov, V., Wolf, D., Phillpot, S. R., Gleiter, H., Deformation twinning in nanocrystalline Al by molecular-dynamics simulation, *Acta Materialia*, **50** (2002) 5005-5020.

[38] Zhang, T., Zhou, K., Chen, Z. Q., Strain rate effect on plastic deformation of nanocrystalline copper investigated by molecular dynamics, *Materials Science and Engineering: A*, **648** (2015) 23-30.

[39] Cao, A., Wei, Y., Atomistic simulations of crack nucleation and intergranular fracture in bulk nanocrystalline nickel, *Physical Review B*, **76** (2007) 024113.

[40] Kitamura, T., Yashiro, K., Ohtani, R., Atomic Simulation on Deformation and Fracture of Nano-Single Crystal of Nickel in Tension, *JSME International Journal Series A Solid Mechanics and Material Engineering*, **40** (1997) 430-435.

[41] Sansoz, F., Dupont, V., Nanoindentation and plasticity in nanocrystalline Ni nanowires: A case study in size effect mitigation, *Scripta Materialia*, **63** (2010) 1136-1139.

[42] Chen, D., Structural modeling of nanocrystalline materials, *Computational Materials Science*, **3** (1995) 327-333.

[43] Li, J., AtomEye: an efficient atomistic configuration viewer, *Modelling and Simulation in Materials Science and Engineering*, **11** (2003) 173.

[44] Plimpton, S., Fast parallel algorithms for short-range molecular dynamics, *Journal of Computational Physics*, **117** (1995) 1-19.

[45] Mendelev, M. I., Kramer, M. J., Hao, S. G., Ho, K. M., Wang, C. Z., Development of interatomic potentials appropriate for simulation of liquid and glass properties of NiZr2 alloy, *Philosophical Magazine*, **92** (2012) 4454-4469.

[46] Wilson, S. R., Mendelev, M. I., Anisotropy of the solid–liquid interface properties of the Ni–Zr B33 phase from molecular dynamics simulation, *Philosophical Magazine*, **95** (2015) 224-241.

[47] Stukowski, A., Visualization and analysis of atomistic simulation data with OVITO–the Open Visualization Tool, *Modelling and Simulation in Materials Science and Engineering*, **18** (2009) 015012.

[48] Kelchner, C. L., Plimpton, S. J., Hamilton, J. C., Dislocation nucleation and defect structure during surface indentation, *Physical Review B*, **58** (1998) 11085.

[49] Stukowski, A., Structure identification methods for atomistic simulations of crystalline materials, *Modelling and Simulation in Materials Science and Engineering*, **20** (2012) 045021.

[50] Juslin, N., Jansson, V., Nordlund, K., Simulation of cascades in tungsten–helium, *Philosophical Magazine*, **90** (2010) 3581-3589.

[51] Stukowski, A., Bulatov, V. V., Arsenlis, A., Automated identification and indexing of dislocations in crystal interfaces, *Modelling and Simulation in Materials Science and Engineering*, **20** (2012) 085007.

[52] Schäfer, J., Albe, K., Competing deformation mechanisms in nanocrystalline metals and alloys: Coupled motion versus grain boundary sliding, *Acta Materialia*, **60** (2012) 6076-6085.

[53] Cheng, Y., Mrovec, M., Gumbsch, P., Crack nucleation at the $\Sigma 9(2-21)$symmetrical tilt grain boundary in tungsten, *Materials Science and Engineering: A*, **483** (2008) 329-332.

[54] Farkas, D., Van Swygenhoven, H., Derlet, P. M., Intergranular fracture in nanocrystalline metals, *Physical Review B*, **66** (2002) 060101.

[55] Frederiksen, S. L., Jacobsen, K. W., Schiøtz, J., Simulations of intergranular fracture in nanocrystalline molybdenum, *Acta Materialia*, **52** (2004) 5019-5029.

[56] Barrett, C. D., Tschopp, M. A., El Kadiri, H., Automated analysis of twins in hexagonal close-packed metals using molecular dynamics, *Scripta Materialia*, **66** (2012) 666-669.

[57] Sun, Z., Van Petegem, S., Cervellino, A., Durst, K., Blum, W., Van Swygenhoven, H., Dynamic recovery in nanocrystalline Ni, *Acta Materialia*, **91** (2015) 91-100.

[58] Geist, D., Gammer, C., Rentenberger, C., Karnthaler, H. P., Sessile dislocations by reactions in NiAl severely deformed at room temperature, *Journal of alloys and compounds*, **621** (2015) 371-377.

[59] Kawabata, T., Takezono, Y., Kanai, T., Izumi, O., Bend tests and fracture mechanism of TiAl single crystals at 293–1073 K. *Acta Metallurgica*, **36** (1988) 963-975.

[60] Guo, P., Qian, L., Meng, J., Zhang, F., Li, L., Low-cycle fatigue behavior of a high manganese austenitic twin-induced plasticity steel, *Materials Science and Engineering: A*, **584** (2013) 133-142.